



# Non-linear Topographic Effects in Two-Layer Flows

Peter G. Baines<sup>1</sup> and Edward R. Johnson<sup>2\*</sup>

<sup>1</sup> Department of Infrastructure Engineering, The University of Melbourne, Melbourne, VIC, Australia, <sup>2</sup> Department of Mathematics, University College London, London, UK

## OPEN ACCESS

### Edited by:

Miguel A. C. Teixeira,  
University of Reading, UK

### Reviewed by:

Paulina Wong,  
The University of Hong Kong,  
Hong Kong  
Qingfang Jiang,  
United States Naval Research  
Laboratory, USA  
Vanda Grubisic,  
National Center for Atmospheric  
Research, USA

### \*Correspondence:

Edward R. Johnson  
e.johnson@ucl.ac.uk

### Specialty section:

This article was submitted to  
Atmospheric Science,  
a section of the journal  
Frontiers in Earth Science

**Received:** 31 August 2015

**Accepted:** 15 January 2016

**Published:** 09 February 2016

### Citation:

Baines PG and Johnson ER (2016)  
Non-linear Topographic Effects in  
Two-Layer Flows.  
Front. Earth Sci. 4:9.  
doi: 10.3389/feart.2016.00009

We consider the nature of non-linear flow of a two-layer fluid with a rigid lid over a long obstacle, such that the flow may be assumed to be hydrostatic. Such flows can generate hydraulic jumps upstream, and the model uses a new model of internal hydraulic jumps, which results in corrections to flows that have been computed using earlier models of jumps that are now known to be incorrect. The model covers the whole range of ratios of the densities of the two fluids, and is not restricted to the Boussinesq limit. The results are presented in terms of flow types in various regions of a Froude number-obstacle height ( $F_0-H_m$ ) diagram, in which the Froude number  $F_0$  is based on the initial flow conditions. When compared with single-layer flow, and some previous results with two layers, some surprising and novel patterns emerge on these diagrams. Specifically, in parts of the diagram where the flow may be supercritical ( $F_0 > 1$ ), there are regions where hysteresis may occur, implying that the flow may have two and sometimes three multiple flow states for the same conditions (i.e., values of  $F_0$  and  $H_m$ ).

**Keywords:** 2-layer flow, non-Boussinesq, topography, Froude number, hydraulic jump

## INTRODUCTION

Some phenomena in the lower atmosphere may be approximately described by motion of a dense lower layer surmounted by a deep upper layer of approximately uniform density. The processes that occur in such flows can be described by the analysis of flows consisting of two layers of uniform density and velocity with a rigid upper surface. This constitutes the simplest form of density-stratified flow, and contains a number of phenomena that are prominent in more complex flows, such as hydraulic jumps. Here we report results of a study of two-layer stratified flow over isolated topography that incorporate some recent results on hydraulic jumps, namely improved (and justifiably correct) models of such jumps, for all density ratios. The Boussinesq approximation (namely, that the fluid density is assumed uniform except where multiplied by  $g$ ) is not made here. This enables a better appreciation of the effects of density variation, particularly in hydraulic jumps. The presence of the upper boundary provides some simplifications, and while not being particularly relevant to the atmosphere, can be removed to an arbitrarily high level.

A general description of two-layer flows over topography is given in Chapter 3 (specifically, Section 3.6 of Baines, 1995, 1998), using models of hydraulic jumps that were prevalent at that time. The cases considered were those of two-layer flow with uniform velocity that commenced from a state of rest over an isolated, long obstacle, and concentrated on the “Boussinesq limit” where the density difference is very small. The resulting flows were described in terms of the parameters  $r$ ,  $F_0$ , and  $H_m$ , where (generalizing to all densities)

$$r = \frac{d_{10}}{D}, H_m = \frac{h_m}{d_{10}}, F_0 = \frac{U}{c_0}, c_0^2 = \frac{\Delta\rho g}{\frac{\rho_1}{d_{10}} + \frac{\rho_2}{d_{20}}}, \quad (1.1)$$

where  $\rho_1$  and  $\rho_2$  denote the lower and upper layer densities respectively,  $\Delta\rho = \rho_1 - \rho_2$ ,  $U$  is the initial fluid velocity in the frame of the obstacle,  $D$  the total depth,  $g$  gravity,  $d_{10}$  and  $d_{20} = D - d_{10}$  the initial undisturbed lower and upper layer thicknesses, and  $h_m$  is the height of the highest point of the obstacle.  $c_0$  denotes the speed of long waves in two-layer fluid at rest. A definition sketch with velocities given in the frame of the topography is given in **Figure 1**. If the lower layer is thinner than the upper layer, the sudden onset of flow generates an hydraulic jump upstream, and the appropriate solutions for the flow depend on the dynamical properties of such jumps.

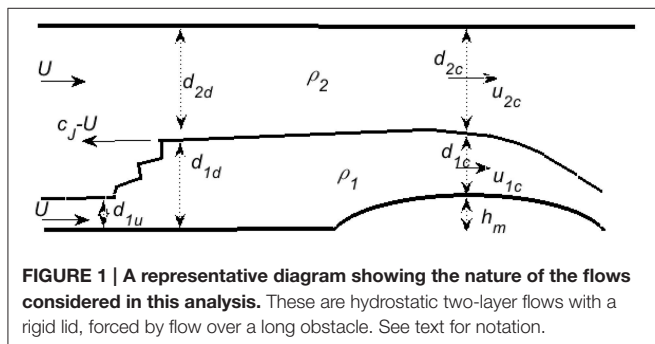
Section Hydraulic Jumps in Two-layer Flows gives a summary of the properties of such jumps based on recent analysis by Borden and Meiburg (2013) for Boussinesq flows, which have been generalized to all densities by the first author of this paper in Baines (2015). A study of jumps in continuously stratified fluids in the Boussinesq limit has been described by White and Helfrich (2014) using the Dubreil-Jacotin-Long equations, which provides an interesting contrast to the two-layer model employed here.

The basic equations for time-dependent non-linear two-layer flow are presented in Section Equations for Time-Dependent Non-linear Two-Layer Flow, and using the new model of hydraulic jumps, the methodology for computing the properties of flow over a single obstacle is presented in Section Two-Layer Flow over a Single Obstacle. The results are given in terms of  $F_0 - H_m$  diagrams in Section Results, and the conclusions are summarized in Section Conclusions.

Flows close to the Boussinesq limit are more relevant to applications to the atmosphere and ocean, where (potential) densities do not vary greatly, and these have been more closely studied in the past, but non-Boussinesq flows show some interesting differences. Flows where the lower layer is thinner than the upper are perhaps the most relevant to atmospheric and oceanic situations, and these are found to be the more complex in the non-Boussinesq case. The new hydraulic jump model may be extended to include mixing within (or downstream of) the jump, and hence also applied to flow over topography, but this has not been done here.

## HYDRAULIC JUMPS IN TWO-LAYER FLOWS

This section summarizes the results given in Baines (2015). An hydraulic jump in two-layer fluids is here defined to be a



flow structure that represents a transition between two steady uniform two-layer flow states (this may be extended to include an undular bore that leaves a downstream wavetrain, in which case the downstream flow state is taken to be the average layer thickness and velocities). A definition sketch for jumps is shown in **Figure 2**, which shows variables and velocities in the frame of the jump: subscripts 1 and 2 denote the lower and upper layers, subscripts “u” and “d” denote upstream and downstream, and  $u$  and  $d$  with subscripts denote layer velocities and thicknesses (see **Figure 1**).  $p_{su}$  and  $p_{sd}$  denote the pressure at the upper surface upstream and downstream respectively. Our objective is to obtain the flow properties downstream of the jump in terms of its amplitude, where the latter is measured by the increment in lower-layer thickness. We make the following assumptions: (1) the jump is steady in a reference frame moving with it; (2) the top and bottom surfaces are horizontal through the jump, with no surface stress, and (3) the layers maintain their identity through the jump, with negligible exchange of fluid between them. With these assumptions we have

$$d_{1u} + d_{2u} = D = d_{1d} + d_{2d}, d_{id}u_{id} = d_{iu}u_{iu}, i = 1, 2. \quad (2.1)$$

and from assumption (2) we have that the momentum flux  $S$  must be uniform (see Baines, 1995, 1998), so that

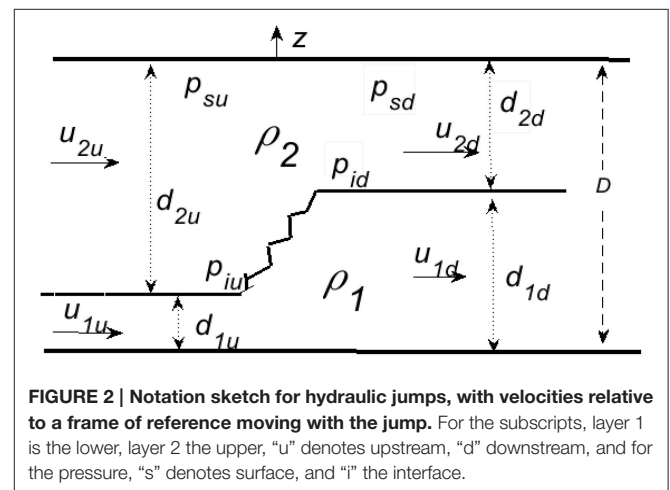
$$S = \int_0^D (p + \rho u^2) dz = \text{constant} \quad (2.2)$$

$$= p_{su}D + \frac{1}{2}\Delta\rho g d_{1u}^2 + \rho_1 u_{1u}^2 d_{1u} + \rho_2 u_{2u}^2 d_{2u} + \frac{1}{2}\rho_2 g D^2,$$

which is equal to the same expression on the downstream side. This equation introduces an additional variable,  $p_{su} - p_{sd}$ , which needs to be determined by other considerations:

$$p_{su} - p_{sd} = \frac{\Delta\rho g}{2D} (d_{1d}^2 - d_{1u}^2) + \rho_1 (u_{1d}^2 d_{1d} - u_{1u}^2 d_{1u}) / D + \rho_2 (u_{2d}^2 d_{2d} - u_{2u}^2 d_{2u}) / D. \quad (2.3)$$

There have been essentially three previous attempts which have involved assumptions about the dynamics to give expressions for



$p_{su}-p_{sd}$ . The first was by Yih and Guha (1955) (the problem is 60 years old!), who assumed that the flow within the jump was hydrostatic, and that  $p_s$  varies linearly with  $d_2$ ; the second was by Chu and Baddour (1977) and Wood and Simpson (1984), who assumed that all the energy dissipation in the jump was contained within the expanding (lower) layer, and the third was by Klemp et al. (1997), who assumed that all the energy dissipation was contained in the contracting (upper) layer. These assumptions gave different results, and with hindsight, none of them is correct, though as it turns out, the model of Klemp et al. is a good approximation in the Boussinesq limit. See Baines (2015) for details.

The novel approach from Borden and Meiburg (2013) was to consider a vorticity budget of the jump, and show, for the Boussinesq case, that the vorticity generation is independent of the pressure difference across the jump, and Equation (2.3) is not needed. In the non-Boussinesq case (Baines, 2015), the vorticity generated is determined by this pressure difference, and provides an expression for it. Specifically, if the vorticity equation (without friction) is written in the form

$$\mathbf{u} \cdot \nabla \omega = -\nabla x \left( \frac{1}{\rho} \nabla p \right), \quad (2.4)$$

and integrated over the area  $A$  of the jump, using the Gauss and Stokes theorems it reduces to

$$\int \omega \mathbf{u} \cdot d\mathbf{S} = - \int \frac{1}{\rho} \nabla p \cdot d\mathbf{l}, \quad (2.5)$$

where  $\mathbf{S}$  denotes the normal vector to the boundary of  $A$ , and  $\mathbf{l}$  denotes the vector along it, in the anti-clockwise sense. Since the density is uniform in each layer, and if  $u_{1u} = u_{2u}$ , this equation reduces to

$$\begin{aligned} \frac{1}{2} (u_{2d}^2 - u_{1d}^2) &= \left[ \frac{1}{\rho_2} - \frac{1}{\rho_1} \right] (p_{iu} - p_{id}) \\ &= \frac{\Delta \rho}{\rho_1} \frac{p_{su} - p_{sd}}{\rho_2} + \frac{\Delta \rho g}{\rho_1} (d_{1d} - d_{1u}), \end{aligned} \quad (2.6)$$

where  $p_{id}$  and  $p_{iu}$  denote the pressures at the downstream and upstream interfaces respectively, which may be related hydrostatically to the surface pressures. This analysis obviates the necessity for the various different assumptions made or proposed by Yih and Guha (1955), Wood and Simpson (1984), Klemp et al. (1997) and Li and Cummins (1998).

From Equations (2.3) and (2.6) we may eliminate  $p_{su} - p_{sd}$ , and obtain the expression for the speed  $c_j$  of an hydraulic jump (see Figure 1) moving into fluid at rest:

$$\left( \frac{c_j}{c_0} \right)^2 = \frac{r_d^2 (1 - r_d)^2 \left[ 1 - r_u \left( 1 - \frac{\rho_2}{\rho_1} \right) \right] \left[ 1 + \left( \frac{\rho_1}{\rho_2} - 1 \right) \frac{(r_u + r_d)}{2} \right]}{r_u (1 - r_u) \left[ \frac{(r_u + r_d)}{2} - r_u r_d + \left( \frac{\rho_1}{\rho_2} - 1 \right) r_u r_d (1 - r_d)^2 - \left( 1 - \frac{\rho_2}{\rho_1} \right) r_d^2 (1 - r_u) (1 - r_d) \right]}, \quad (2.7)$$

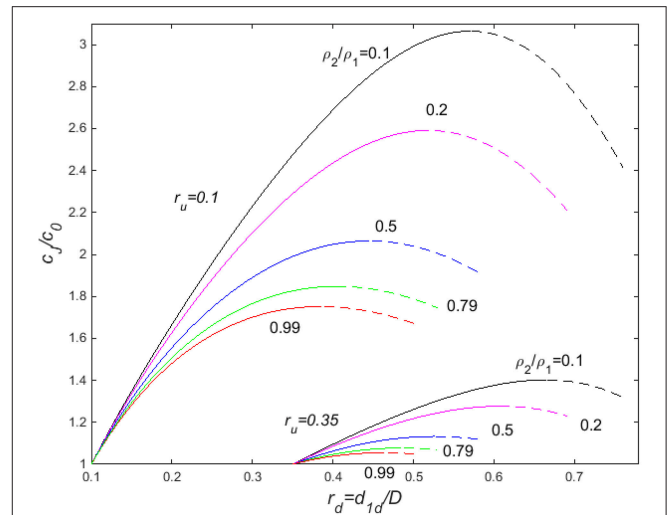


**FIGURE 3 | Some representative jump speeds as a function of jump amplitude, moving into fluid at rest, for a range of density ratios ( $\rho_2/\rho_1 = 0.1, 0.2, 0.5, 0.79, 0.99$ ). The upstream lower layer thicknesses are given by  $r_u = d_{1u}/D = 0.1$  and  $0.35$ . The dashed portions of the curves denote the regions where jump speed decreases with increasing amplitude. This makes them potentially unstable. Further, for these dashed curves, the flow is supercritical (relative to the jump) on the downstream side. This means that disturbances from downstream cannot propagate up to the jump and increase (or affect) it. In particular, jumps with amplitude greater than that of maximum speed cannot be generated from downstream, so that only the solid parts of the curves represent enduring jumps generated by flow over topography.**

where  $c_0$  is the linear wavespeed as in Equation (1.1) and  $r_u = d_{1u}/D$ ,  $r_d = d_{1d}/D$ . Borden and Meiburg (2013) termed their Boussinesq model for the jump speed the VS, or “Vortex Sheet” model, so that it is appropriate to term this model the FVS, or “Full Vortex Sheet” model.

Some representative plots for  $c_j/c_0$  are shown in Figure 3, as a function of  $r_d$ , for a range of density ratios. Note that all of these curves attain a maximum speed, but exist at larger amplitude, up to a maximum amplitude where the energy loss in each layer vanishes. For each curve, the maximum energy loss in each layer within the jump coincides with the point of maximum speed. Further, relative to the reference frame of the jump, the flow immediately downstream is subcritical for jump amplitudes  $r_d$  less than that of maximum speed (denoted  $r_{dms}$ ), but is supercritical for jumps with amplitudes greater than or equal to that maximum speed ( $r_d \geq r_{dms}$ ). This means that, on the dashed part of the curves, disturbances from downstream cannot propagate up to these jumps and affect them. Such jumps, if they did exist, would also be expected to be unstable, and degenerate to a jump of maximum speed. For these reasons, the jumps with  $r_d \geq r_{dms}$  are shown dashed in Figure 3, and are not significant in the following analysis. More details are given in Baines (2015).

Observations of the speeds of hydraulic jumps in two-layer flows with water and kerosene ( $\rho_2/\rho_1 = 0.79$ ) forced by flow over (under) an obstacle were measured by Baines (1984), and at the time were compared with the model of Yih and Guha (1955). The agreement was somewhat disappointing. Comparisons between the same observations and jump speeds from the current model described above are shown in **Figure 4**, and the agreement is much more satisfying (see Baines, 2015 for a comparison with Yih and Guha). This lends support to the notion that this new model is indeed the correct formulation for two-layer hydraulic jumps.

### EQUATIONS FOR TIME-DEPENDENT NON-LINEAR TWO-LAYER FLOW

We now consider two-layer flow over a long obstacle for which the horizontal length scale  $L$  and the time scale of the motion are sufficiently large for the equation for vertical motion to be hydrostatic, apart from the possible presence of hydraulic jumps. Under these conditions the equations of motion for the two layers may be written

$$\frac{\partial u_1}{\partial t} + \frac{\partial}{\partial x} \left[ \frac{1}{2} u_1^2 + g \left( h + d_1 + \frac{\rho_2}{\rho_1} d_2 \right) + \frac{p_s}{\rho_1} \right] = 0, \quad (3.1)$$

$$\frac{\partial u_2}{\partial t} + \frac{\partial}{\partial x} \left[ \frac{1}{2} u_2^2 + g (h + d_1 + d_2) + \frac{p_s}{\rho_2} \right] = 0, \quad (3.2)$$

where  $u_1, u_2, d_1, d_2$  denote the velocities and thicknesses of layers 1 and 2, and  $h(x)$  is the height of any bottom topography on the lower surface. If the upper layer has a rigid upper surface, and we assume that the total flow of fluid through the system is constant, we have, at all locations  $x$ ,

$$h(x) + d_1 + d_2 = D, \quad d_1 u_1 + d_2 u_2 = Q, \quad (3.3)$$

where  $Q$  is the nett volume flux through the system, presumed constant after some initial starting time  $t = t_0$ . This system of equations governs the internal or baroclinic mode, and may be reduced to two equations for two convenient perturbation variables  $v$  and  $\eta$ , defined by

$$v = u_1 - \frac{\rho_2}{\rho_1} u_2, \quad d_1 + h = d_{10} + \eta, \quad d_2 = d_{20} - \eta, \quad (3.4)$$

where  $d_{10}$  and  $d_{20}$  denote a reference state for the thicknesses  $d_1$  and  $d_2$ . If the unknown surface pressure  $p_s$  is eliminated by subtraction, from the above we may obtain equations for  $v$  and  $\eta$  in the form

$$\frac{\partial \eta}{\partial t} + \frac{\partial}{\partial x} \left[ \frac{(d_{20} - \eta)(d_{10} - h + \eta)v + \frac{1}{2}Q \left( \eta - d_{20} + \frac{\rho_2}{\rho_1}(d_{10} - h + \eta) \right)}{D - h - \delta} \right] = 0, \quad (3.5)$$

$$\frac{\partial v}{\partial t} + \frac{\partial}{\partial x} \left[ \frac{\Delta \rho g \eta}{\rho_1} + \frac{\left[ (d_{20} - \eta)^2 - \frac{\rho_2}{\rho_1}(d_{10} - h + \eta)^2 \right] v^2 + \frac{\rho_2}{\rho_1} \left[ 2Qv(D - h) - \left( 1 - \frac{\rho_2}{\rho_1} \right) Q^2 \right]}{2(D - h - \delta)^2} \right] = 0, \quad (3.6)$$

where

$$\delta = \frac{\Delta \rho}{\rho_1} (d_{10} - h + \eta). \quad (3.7)$$

These equations describe time-dependent motions in this two-layer system, which involve waves on the interface. There are two waves, propagating in opposite directions relative to the mean motion of the local fluid, and these waves may be described by the characteristic equations as follows (e.g., Whitham, 1974).

Equations (3.6–7) may be expressed as

$$\frac{\partial \eta}{\partial t} + a_{11} \frac{\partial \eta}{\partial x} + a_{12} \frac{\partial v}{\partial x} = b_1 \frac{\partial h}{\partial x}, \quad \frac{\partial v}{\partial t} + a_{21} \frac{\partial \eta}{\partial x} + a_{22} \frac{\partial v}{\partial x} = b_2 \frac{\partial h}{\partial x}, \quad (3.8)$$

where  $a_{11}(\eta, v)$  etc. are given in the Appendix, and in the region where  $h = 0$ , we may (trivially) write, for any arbitrary factors  $l_1, l_2$ ,

$$l_1 \left( \frac{\partial \eta}{\partial t} + a_{11} \frac{\partial \eta}{\partial x} + a_{12} \frac{\partial v}{\partial x} \right) = 0, \quad l_2 \left( \frac{\partial v}{\partial t} + a_{21} \frac{\partial \eta}{\partial x} + a_{22} \frac{\partial v}{\partial x} \right) = 0. \quad (3.9)$$

If we may write

$$l_1 a_{11} + l_2 a_{21} = l_1 c, \quad l_1 a_{12} + l_2 a_{22} = l_2 c, \quad \text{which requires} \\ \det [a_{ij} - cI] = 0, \quad (3.10)$$

for real values of  $c$ , adding the two equations in Equation (3.9) gives

$$l_1 \left( \frac{\partial \eta}{\partial t} + c \frac{\partial \eta}{\partial x} \right) + l_2 \left( \frac{\partial v}{\partial t} + c \frac{\partial v}{\partial x} \right) = 0, \quad \text{i.e., } l_1 \frac{d\eta}{dt} + l_2 \frac{dv}{dt} = 0, \quad (3.11)$$

where

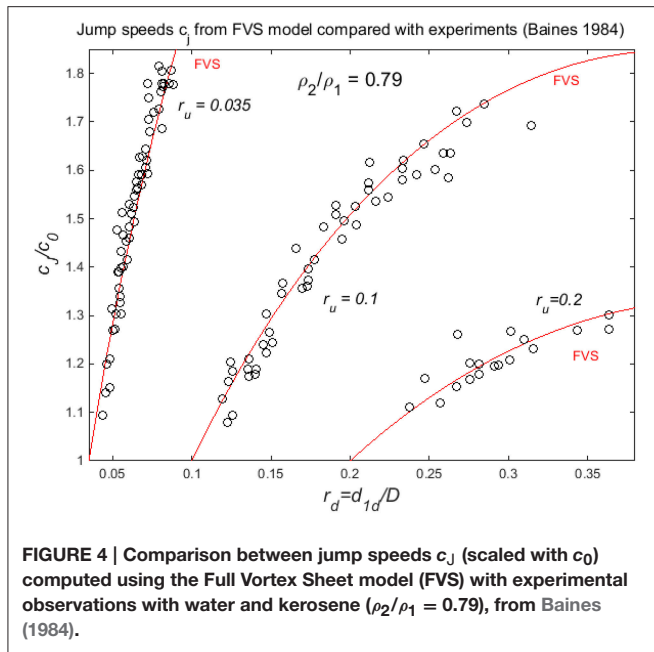
$$\frac{d}{dt} (\eta, v) = \frac{\partial}{\partial t} (\eta, v) + c \frac{\partial}{\partial x} (\eta, v). \quad (3.12)$$

There are two solutions for  $c$ , denoted  $c_+$  and  $c_-$ , for waves propagating rightward (with the stream  $c_+$ ), and leftward, against it ( $c_-$ ). It follows that the time-dependent motion at a given point is the sum of the leftward- and rightward-propagating motions with speeds given by Equation (3.10), which are

$$c_+, c_- = \frac{1}{2} (a_{11} + a_{22}) \pm \frac{1}{2} \left[ (a_{11} - a_{22})^2 + 4a_{21}a_{12} \right]^{1/2}. \quad (3.13)$$

### TWO-LAYER FLOW OVER A SINGLE OBSTACLE

We consider motions governed by the above equations, with the initial conditions:



$$u_1 = u_2 = U, d_1 = d_{10} + h(x), d_2 = d_{20} - h(x), att = 0, \quad (4.1)$$

after which  $U$  and  $h(x)$  remain constant. This corresponds to the sudden introduction of the obstacle into a uniform two-layer stream (the result is similar to that for the sudden onset of a uniform two-layer stream over a stationary obstacle). Our objective is to describe the properties of the resulting flow in terms of the parameters given in Equation (1.1).

For a sufficiently small obstacle, the commencement of conditions Equation (4.1) causes two transient disturbances, each having the form of the topography. One of these propagates against the flow, and the other with it, as described in Section Equations for Time-Dependent Non-linear Two-layer Flow, leaving a locally steady solution in the vicinity of the obstacle. This steady solution is given by steady forms of Equations (3.5) and (3.6), where the square-bracket terms are equal to their values where  $h, \eta,$  and  $v = 0$ . They may also be manipulated to give the “hydraulic alternative,” namely that

$$\frac{d}{dx} (\eta, v) = 0, \text{ or } c_- = 0, \text{ where } \frac{dh}{dx} = 0. \quad (4.2)$$

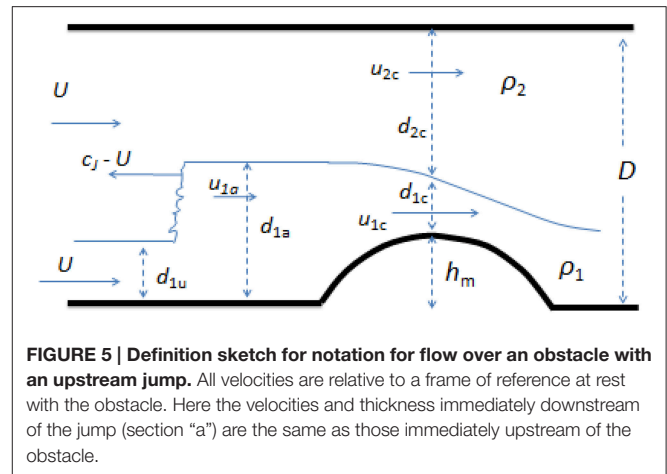
If  $c_- < 0$  the flow is subcritical, and if both  $c_+, c_- > 0$  the flow is supercritical, and the steady solution applies provided  $c_- \neq 0$ , which implies  $F_0 \neq 1$ .

For subcritical flows where  $r_u = d_{10}/D$  is small, as  $H_m$  is increased the steady solution is valid until a point is reached at which  $c_- = 0$  at the peak of the obstacle, i.e.,

$$c_- = \frac{1}{2} (a_{11} + a_{22}) - \frac{1}{2} [(a_{11} - a_{22})^2 + 4a_{21}a_{12}]^{1/2}, \quad (4.3)$$

where  $a_{ij}$  are given in the Appendix with

$$d_1 = d_{11}, d_2 = d_{21}, \eta = \eta_c, v = v_c, h = h_m, \quad (4.4)$$



$\eta_c$  and  $v_c$  denoting the values of  $\eta$  and  $v$  at the critical section at the peak of the obstacle.

For larger heights the steady solution is not valid, and the fluid responds by sending a disturbance upstream, which effectively alters the upstream flow conditions. The flow over the obstacle is then no longer symmetric about the highest point, and for the resulting steady flow, the fluid must adjust so that the second alternative— $c_- = 0$  applies there. Further increases in the obstacle height beyond this point cause yet faster disturbances to propagate upstream, with the result that the flow forms upstream hydraulic jumps. When this happens, it is necessary to take into account the properties of hydraulic jumps, and assuming steady flow over the obstacle, to link this to the condition  $c_- = 0$  at the obstacle crest. The appropriate variables and notation are shown in **Figure 5**. The new (correct) formulation for hydraulic jumps described in Section Hydraulic Jumps in Two-layer Flows above is used here. The simplest procedure is to assume a given upstream jump height, and then take the conditions downstream of the jump as input to flow over the topography, where the critical condition at the obstacle crest together with the steady-state forms of Equations (3.5) and (3.6) determines the obstacle height. From this one may construct regions of the  $F_0-H_m$  diagram. For subcritical flows with small  $r_u$ , the above phenomena are sufficient to describe the upstream flow properties up to the point where the lower layer becomes blocked by the topography, and is locally absent on the downstream side.

The above procedure is essentially the same as that for single-layer flows over obstacles (e.g., Baines, 1995, 1998, Section 2.3). But for larger values of  $r_u$ , and supercritical flows, increasing  $H_m$  may cause the upstream jump to reach its maximum speed. At this point, the flow immediately downstream of the upstream jump becomes supercritical, as described in Section Hydraulic Jumps in Two-layer Flows. This means that, although larger-amplitude jumps are theoretically possible, they cannot be built up by disturbances approaching it from the downstream side, and hence the flow must respond in some other way. Increasing  $H_m$  causes more upstream disturbances that increase the lower layer thickness and progressively travel

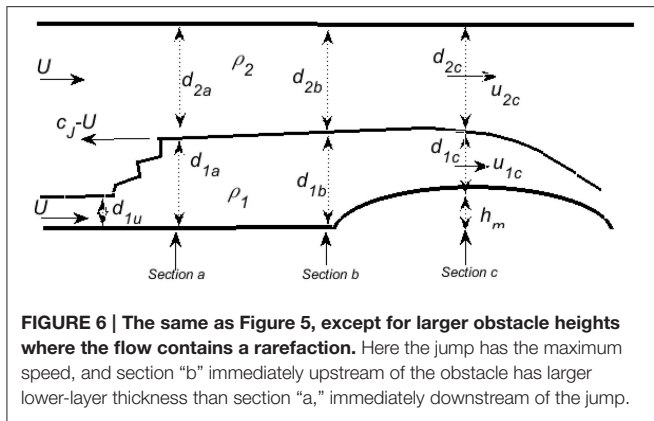


**FIGURE 6 | The same as Figure 5, except for larger obstacle heights where the flow contains a rarefaction.** Here the jump has the maximum speed, and section “b” immediately upstream of the obstacle has larger lower-layer thickness than section “a,” immediately downstream of the jump.

more slowly, so that the resulting upstream disturbance becomes more spread out as it propagates, rather than steepening to form an hydraulic jump. Such a disturbance is termed a *rarefaction*, because the disturbance itself is becoming more rarefied with time (see Chapter 3 of Baines, 1995, 1998). The resulting upstream motions are governed by Equations (3.8–12), and the flow has the form shown in **Figure 6**. The flow eventually reaches a quasi-steady form, with the distance between the jump and the obstacle progressively increasing, but with a dynamical link between them manifested in the interfacial waves. The only way the jump can influence the flow downstream is via the rightward-propagating waves (with speed  $c_+$ ).

The rightward propagating waves commence with the conditions at section *a* of **Figure 6**, immediately downstream of the jump. With  $c = c_+$ , Equation (3.11) provides the relation

$$\frac{dv}{d\eta} = -\frac{l_1}{l_2} = -\frac{a_{11} - a_{22} \pm [(a_{11} - a_{22})^2 + 4a_{21}a_{12}]^{1/2}}{2a_{12}}, \quad (4.5)$$

where the plus sign is taken. This gives a relation between  $v$  and  $\eta$  for these downstream propagating waves. The expressions for  $a_{11}(\eta, v)$  etc. are those given in the Appendix, with  $d_1 = d_{11}$ ,  $d_2 = d_{21}$ , and the initial conditions of section *a*:

$$\eta = 0, v = u_{11} - \frac{\rho_2}{\rho_1} u_{21}, \quad (4.6)$$

where  $u_{11}, u_{21}$  are the velocities at Section Introduction in the frame of the obstacle, and are determined by the properties of the jump. Integrating Equation (4.3) then gives a relation between  $v$  and  $\eta$  that applies up to section *b* of **Figure 6**, immediately upstream of the obstacle.

The jump equations give the conditions ( $v$  and  $\eta$ ) downstream of the jump at section *a*, and Equation (4.3) links these conditions with those upstream of the obstacle at section *b*. The steady-state forms of Equations (3.5) and (3.6) and the critical condition at the obstacle crest then give the obstacle height, as before. For clarity, we here describe this process in a little more detail.

In general, Equation (4.3) must be integrated numerically using the expressions in the Appendix, where  $d_1, d_2$  denote the layer thicknesses immediately downstream of the jump. In the notation of **Figure 5**, the initial conditions at section *a* are therefore

$$d_1 = d_{1a}, d_2 = d_{2a}, \eta_a = 0, v_a = u_{1a} - \frac{\rho_2}{\rho_1} u_{2a}, \quad (4.7)$$

and Equation (4.5) gives a relationship between  $v$  and  $\eta$ . It should be noted that Section Introduction is not at a fixed location, but the velocities in Equation (4.7) are relative to the reference frame of the obstacle, as in **Figure 5**.

In the Boussinesq limit, the  $a_{ij}$  take the form

$$a_{11} = \frac{v(d_2 - d_1 + h - 2\eta) + Q}{D - h}, \quad (A.11)$$

$$a_{12} = \frac{(d_2 - \eta)(d_1 - h + \eta)}{D - h}, \quad (A.11)$$

$$a_{21} = \frac{\Delta\rho g}{\rho_1} - \frac{v^2}{D - h}, a_{22} = a_{11}, \quad (A.12)$$

so that Equation (4.5) can be expressed as

$$\frac{dv}{d\eta} = -\left(\frac{a_{21}}{a_{12}}\right)^{1/2} = -\left(\frac{g'D - v^2}{(d_{2a} - \eta)(d_{1a} + \eta)}\right)^{1/2}, \quad (4.8)$$

where  $g' = \frac{\Delta\rho g}{\rho_0}$ .

Equation (4.8) can then be integrated directly to give the “Riemann invariant”

$$\arcsin\left(\frac{2\eta + d_{1a} - d_{2a}}{D}\right) + \arcsin\left(\frac{v}{(g'D)^{1/2}}\right) = \arcsin\left(\frac{d_{1a} - d_{2a}}{D}\right) + \arcsin\left(\frac{u_{1a} - u_{2a}}{(g'D)^{1/2}}\right). \quad (4.9)$$

This gives a relationship between  $v$  and  $\eta$  that applies immediately upstream of the topography (denoted section *b* in **Figure 5**, with variables  $d_{1b}, d_{2b}, u_{1b}, u_{2b}, \eta_b, v_b$ ). The flow over the obstacle may be assumed to be steady after sufficient time has elapsed. We may therefore use the steady-state versions of Equations (3.5) and (3.6) to link the flow immediately upstream of the obstacle to the flow at the obstacle crest (denoted section *c* in **Figure 5**), which for the general case give.

$$\frac{(d_{2a} - \eta_b)(d_{1a} + \eta_b)v_b + \frac{1}{2}Q\left(\eta_b - d_{2a} + \frac{\rho_2}{\rho_1}(d_{1a} + \eta_b)\right)}{D - \delta_b} = \frac{(d_{2a} - \eta_c)(d_{1a} - h_m + \eta_c)v_c + \frac{1}{2}Q\left(\eta_c - d_{2a} + \frac{\rho_2}{\rho_1}(d_{1a} - h_m + \eta_c)\right)}{D - h_m - \delta_c}, \tag{4.10}$$

$$g'\eta_b + \frac{\left[(d_{2a} - \eta_b)^2 - \frac{\rho_2}{\rho_1}(d_{1a} + \eta_b)^2\right]v_b^2 + \frac{\rho_2}{\rho_1}\left[2Qv_bD - \left(1 - \frac{\rho_2}{\rho_1}\right)Q^2\right]}{2(D - \delta_b)^2} = g'\eta_c + \frac{\left[(d_{2a} - \eta_c)^2 - \frac{\rho_2}{\rho_1}(d_{1a} - h_m + \eta_c)^2\right]v_c^2 + \frac{\rho_2}{\rho_1}\left[2Qv_c(D - h_m) - \left(1 - \frac{\rho_2}{\rho_1}\right)Q^2\right]}{2(D - h_m - \delta_c)^2}, \tag{4.11}$$

where  $\delta_b = \frac{\Delta\rho}{\rho_1}(d_{1a} + \eta_b)$ ,  $\delta_c = \frac{\Delta\rho}{\rho_1}(d_{1a} - h_m + \eta_c)$ .  $(4.12)$

The other remaining equation is the critical condition at the obstacle crest, as in Equation (4.3), which takes the form

$$c_- = \frac{1}{2}(a_{11}(\eta_c, v_c, h_m) + a_{22}(\eta_c, v_c, h_m)) - \frac{1}{2}\left[(a_{11}(\eta_c, v_c, h_m) - a_{22}(\eta_c, v_c, h_m))^2 + 4a_{21}(\eta_c, v_c, h_m)a_{12}(\eta_c, v_c, h_m)\right]^{1/2} = 0, \tag{4.13}$$

using the expressions for  $a_{ij}$  in the Appendix, with  $d_1 = d_{1a}$ ,  $d_2 = d_{2a}$ . We therefore have four equations for the four variables  $\eta_b, v_b, \eta_c, v_c$ , for an upstream jump of given amplitude and hence known values of  $d_{1a}, d_{2a}, u_{1a}, u_{2a}, v_a$ , (with  $\eta_a = 0$ ) which enables us to determine the appropriate value of  $h_m$ . Hence one may construct diagrams of flow properties in the  $F_0 - H_m$  plane, for various values of the density ratio  $\rho_2/\rho_1$ . For the situations analyzed for this paper (shown in **Figures 9, 10**), the regions in  $F_0 - H_m$  space where rarefactions occur are small.

### RESULTS

With the above analysis, we may determine the nature of the two-layer flow over an obstacle, and its variation with the relevant parameters. We are concerned with flows that are (or are equivalent to being) started from a state of rest, and after a short starting period are maintained at constant conditions. This includes, for example, an obstacle that is towed through stationary fluid, or a stationary obstacle situated in a two-layer stream where the latter is suddenly forced into uniform motion.

An effective way of getting an overall view of the types of flow that may occur is through the  $F_0 - H_m$  diagram. Here, given uniform initial flow velocity, we have two additional parameters:  $r_u = d_{10}/D$ , the initial relative thickness of the lower layer, and  $\rho_2/\rho_1$ , the ratio of the densities of the fluids in the two layers. We present some representative examples of such diagrams which indicate some surprising and novel features of the flow of two fluids. This includes the phenomenon of “hysteresis,” or multiple steady flow states, in parameter ranges that include the state of fully supercritical flow over the obstacle.

As a point of reference and subsequent comparison, **Figure 7** shows the  $F_0 - H_m$  diagram for a single homogeneous fluid layer (from Baines and Davies, 1980; Baines, 1995, 1998). This shows parameter ranges where the ultimate steady flow is wholly subcritical or supercritical over the obstacle, where the fluid is blocked by the topography, and where the flow over the obstacle forces an upstream jump that alters the approaching flow, which is governed by a critical condition at the crest of the obstacle. There is also a parameter range within which a hysteresis phenomenon may occur. Here the flow over the obstacle may be entirely supercritical, or partially blocked (with an upstream hydraulic jump) with critical flow at the crest: subcritical on the upstream side, and supercritical on the downstream side. Which of these two states occurs in practice will depend on how the flow is set up. One may then make the transition from one state to the other by slowly varying the basic flow parameters  $F_0$  and  $H_m$  in a quasi-static manner—hence the term “hysteresis.”

One may expect similar types of behavior to occur for two-layer flow over topography. Some examples have been

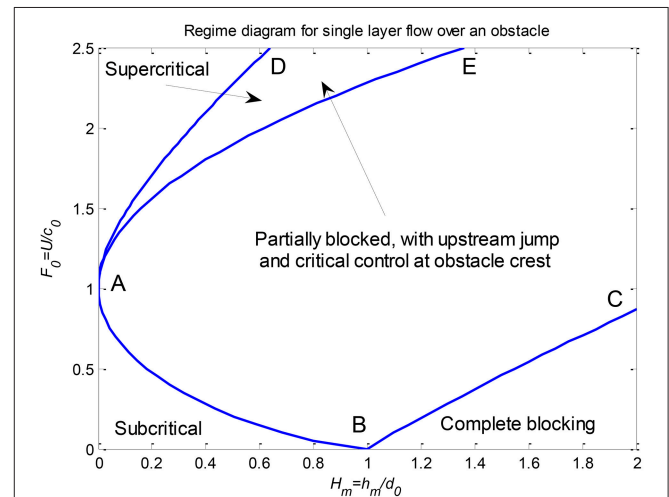


**FIGURE 7 | Regime diagram for hydrostatic single-layer flow over an obstacle.**  $U$  and  $d_0$  are the initial fluid velocity and layer thickness, with  $c_0$  the wavespeed. In the region EABC the flow is partially blocked, with an upstream hydraulic jump controlled by a critical condition at the obstacle crest. DAE is the “hysteresis” region, in which the flow may be either partially blocked as in EABC, or supercritical, as above AD, as indicated by arrows. For more details see Section 2.3 of Baines (1995, 1998).

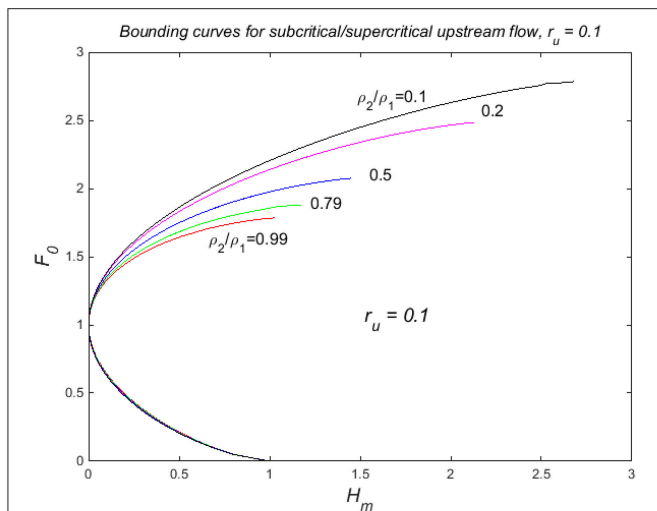


**FIGURE 8 |** Curves for the onset of critical flow at the obstacle crest as  $H_m$  increases from zero, with no upstream jump, for a range of density ratios, for  $r_u = 0.1$ . For  $F_0$  values larger (or  $H_m$  less) than those on the upper part of these curves, the steady flow is everywhere supercritical, and for  $F_0$  (or  $H_m$ ) less than the lower part (where these curves effectively coincide), the steady flow is subcritical.

given by Baines (1984) for the special case of water and kerosene, where a range of parameters with two states was observed experimentally. However, computations for flows in the Boussinesq limit (Baines, 1995, 1998) using the Yih-Guha hydraulic jump model (which seemed to be the best available at the time) did not give any multiple states. Here we present two parameter diagrams in which  $r_u = 0.1$ , and is representative of thin lower layers. In one of these,  $\rho_2/\rho_1$  is small (0.1), and in the other, 0.99, which is very close to the Boussinesq limit. The contrast between these two cases is surprising and instructive. But first, **Figure 8** shows the curves for the boundary of wholly subcritical (for  $F_0 < 1$ ) or wholly supercritical (for  $F_0 > 1$ ) flow as the obstacle height is increased from zero in a stream with given  $F_0$ , for a range of density ratios, for  $r_u = 0.1$ . The positions and shapes of these curves are generally similar in form to that for a single layer, which is curve BAE in **Figure 7**. The main difference is that single-layer curve BAE is unlimited, whereas all the two-layer curves must necessarily terminate.

**Figure 9** shows the  $F_0 - H_m$  diagram for  $r = r_u = 0.1$ ,  $\rho_2/\rho_1 = 0.99$ , near the Boussinesq limit. Here curve BAE denotes the critical flow condition, with subcritical/supercritical flow to the left if  $F_0 < 1/F_0 > 1$ , and partially blocked lower-layer flow with an upstream jump to the right (as in **Figure 7**). The magnitude of this jump is given by the plotted values of  $r_a = d_{1a}/D$ . This part of the diagram extends to the line where  $r_a = 0.385$ , which is the value for the maximum jump speed. The curves terminate at the boundary where the lower layer is completely blocked, and for larger  $F_0$ , there is a small region where larger upstream motions occur through rarefactions. This is limited by the flow immediately upstream of the obstacle becoming critical, which occurs where  $r_b$  is very close to 0.45. For larger values of  $F_0$ , or  $H_m$ , the flow over the obstacle is supercritical.

This figure is similar to Figure 3.12a of (Baines, 1995, 1998), which uses Yih and Guha, as described above except that the

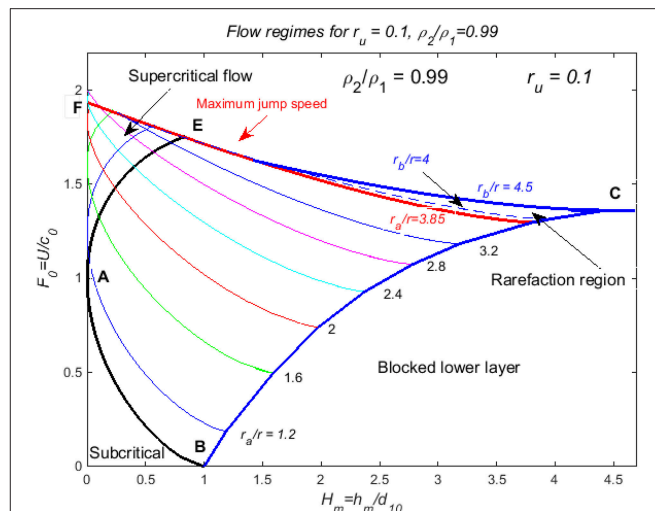
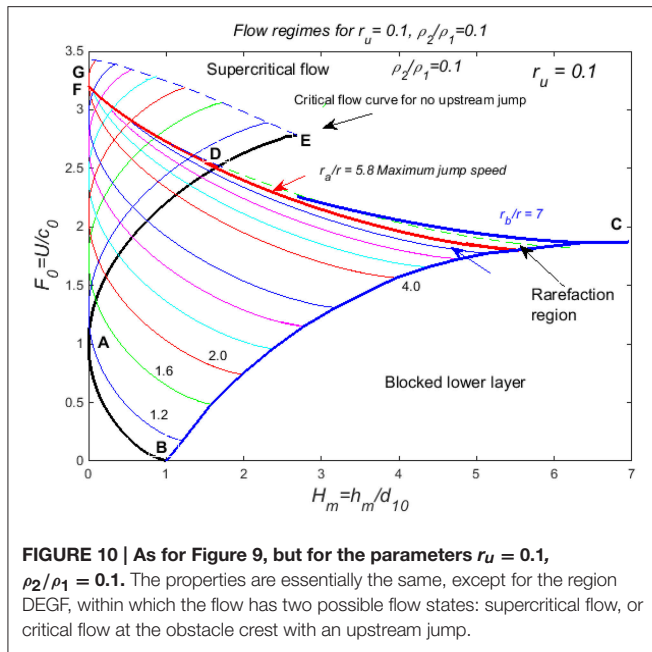


**FIGURE 9 |** Flow properties for steady-state flow over an obstacle, depicted on the  $F_0 - H_m$  diagram for  $r = r_u = 0.1$ ,  $\rho_2/\rho_1 = 0.99$ —the near-Boussinesq case. The flow is subcritical below AB, and upstream hydraulic jumps occur to the right of EAB below EC; the lower layer is completely blocked to the right of BC. Rarefactions that increase the upstream disturbance above that due to the jump of maximum speed occur in the small region immediately below EC, above the curve with  $r_a/r_u = 3.85$ . In the region AEF, there are three possible flow states: supercritical flow, and two states with different upstream jump heights, given by the cross-over of the two curves passing through any given point.

curves for the amplitudes of upstream jumps extend beyond AE. Here, because some of these curves “double back” after touching  $H_m = 0$ , there are two additional solutions for the upstream flow, in the region below the curve for maximum jump speed. Given that the flow in this region may also be supercritical, there are three possible solutions in the region AEF—a jump at small amplitude, a jump at somewhat larger amplitude, and no jump at all (supercritical flow, as indicated by the arrow). It is possible that one or more of these jumps may be unstable, but this has not been investigated.

The  $F_0 - H_m$  diagram for  $r = 0.1$ ,  $\rho_2/\rho_1 = 0.1$  is shown in **Figure 10**. Here the overall pattern is the same as for **Figure 9**, with the exception that the bounding curve BADE for supercritical flow extends above the boundary line FDC for partially blocked flows. In particular there is a region above FD where partially blocked or completely supercritical flows are possible, between DE and the axis  $H_m = 0$ . This is an upward extension of the curves that commence from the line BC. Hence, there are six different regions in this diagram. The first four are: subcritical flow below AB, blocked lower layer below BC, supercritical flow above GEDC, and partially blocked flow with upstream jump in DABCD; in these regions the flow state for given  $(F_0, H_m)$  is unique. In the region ADFA there are three possible flow states: supercritical flow, and two possible critically controlled flows with different upstream jumps, given by the intersecting contours of jump height at any particular point. In section DEGFD the same applies, except that there is only one possible upstream jump. This latter region is curious because, when compared with the diagram for single-layer flows (**Figure 7**), the region with multiple states is to the left of curve ADE, whereas for single-layer flows it is to the right of it.



A corresponding diagram for  $r_u = 0.1$ ,  $\rho_2/\rho_1 = 0.5$  (not shown) displays the same features as in Figure 10, but the region ADFA is less pronounced, so that the diagram is closer to that of Figure 9, as might be expected.

## CONCLUSIONS

We have used a new (and within its limitations, essentially correct) formulation of two-layer hydraulic jumps to determine the properties of non-linear flow over long obstacles. This hydraulic jump formulation uses a vorticity balance to infer the pressure differences across the jump, and avoids assumptions made in earlier models that are now seen to be incorrect. The model can be (and has been) applied to a full range of upstream conditions and density ratios, and hence is not restricted to the

## REFERENCES

- Baines, P. G., and Davies, P. A. (1980). "Laboratory studies of topographic effects in rotating and/or stratified fluids," in *Orographic Effects in Planetary Flows*, GARP Publication No. 23 (World Meteorological Organisation/International Council of Scientific Unions), 233–299.
- Baines, P. G. (1984). A unified description of two-layer flow over topography. *J. Fluid Mech.* 146, 127–167.
- Baines, P. G. (1995, 1998). *Topographic Effects in Stratified Flows*. Cambridge, UK: Cambridge University Press.
- Baines, P. G. (2015). Internal hydraulic jumps in two-layer systems. *J. Fluid Mech.* 787, 1–15. doi: 10.1017/jfm.2015.662
- Borden, Z., and Meiburg, E. (2013). Circulation-based models of Boussinesq internal bores. *J. Fluid Mech.* 276, R1, doi: 10.1017/jfm.2013.239
- Chu, V. H., and Baddour, R. E. (1977). Surges, waves and mixing in two-layer density stratified flow. *Proc. Int. Assn. Hydraul. Res.* 1, 303–310.
- Klemp, J. B., Rotunno, R., and Skamarock, W. C. (1997). On the propagation of internal bores. *J. Fluid Mech.* 331, 81–106.
- Li, M., and Cummins, P. F. (1998). A note on hydraulic theory of internal bores. *Dyn. Atmos. Oceans* 28, 1–7.
- White, B. L., and Helfrich, K. R. (2014). A model for internal bores in continuous stratification. *J. Fluid Mech.* 761, 282–304. doi: 10.1017/jfm.2014.599
- Whitham, G. B. (1974). *Linear and Non-Linear Waves*. New York, NY: J. Wiley & Sons. 636.
- Wood, I. R., and Simpson, J. E. (1984). Jumps in layered miscible fluids. *J. Fluid Mech.* 140, 329–342.
- Yih, C.-S., and Guha, C. R. (1955). Hydraulic jump in a uid system of two layers. *Tellus* 7, 358–366.

Boussinesq limit. For obstacles moving relative to fluid at rest, there are four main dimensionless parameters involved: the lower layer thickness ratio  $r_u = d_{10}/D$ , the density ratio  $\rho_2/\rho_1$ , the initial Froude number  $F_0$ , and the obstacle height ratio  $H_m = h_m/d_{10}$ .

The nature of the resulting flows (steady over the obstacle) has features similar to those obtained with a single layer—sub- or supercritical flow for small obstacle heights for small values of  $H_m$ , and an upstream hydraulic jump followed by a thicker lower layer and governed by a critical condition at the obstacle crest, for larger  $H_m$ . The hydraulic jumps, however, have a maximum speed, and when this is reached, larger amplitude jumps cannot be forced from the topography. Instead, the upstream disturbances forced by larger obstacle heights have the form of rarefactions, which become elongated and lag behind the jump. For  $r_u$  values  $\geq 0.5$ , only rarefactions are present, and previous analysis without jumps is still valid (e.g., Figure 3.12d of Baines, 1995, 1998).

The use of the new hydraulic jump formulation produces some surprises that are best seen in the flow types in the various regions of the  $F_0$ - $H_m$  plane diagrams of Figures 9, 10. These are very different from previous versions (see for example Figures 3.12a,b of Baines, 1995, 1998) which used the jump formulation of Yih and Guha (1955). Figure 9 shows results for  $\rho_2/\rho_1 = 0.99$ , near the Boussinesq limit. Here the surprise is in the “supercritical” region AEF, where in addition to possibly being supercritical, the flow may have two other flow states with upstream jumps, of different heights. In Figure 10, the same phenomenon is seen in region ADE, but now there is an additional region FDEG in which there are two possible states—supercritical flow, or an upstream jump with critical flow at the crest. This region FDEG is vanishingly small for  $\rho_2/\rho_1 = 0.99$ , but increases in size as  $\rho_2/\rho_1$  decreases toward zero.

## AUTHOR CONTRIBUTIONS

This work relies heavily on earlier work by PGB who initiated the present study. ERJ contributed subsequently. Both authors approved it for publication.

**Conflict of Interest Statement:** The authors declare that the research was conducted in the absence of any commercial or financial relationships that could be construed as a potential conflict of interest.

Copyright © 2016 Baines and Johnson. This is an open-access article distributed under the terms of the Creative Commons Attribution License (CC BY). The use, distribution or reproduction in other forums is permitted, provided the original author(s) or licensor are credited and that the original publication in this journal is cited, in accordance with accepted academic practice. No use, distribution or reproduction is permitted which does not comply with these terms.

## APPENDIX

The functions  $a_{ij}, b_i$  in Equation (3.8) take the following general forms. The variable  $\eta$  is relative to layer thicknesses  $d_1, d_2$ , for the lower and upper layers respectively, where  $d_1 + d_2 + h = D$ . With  $d_1$  and  $d_2$  as reference values, for  $a_{ij}(\eta, v)$  we have

$$a_{11} = \frac{v(d_2 - d_1 + h - 2\eta) + \frac{Q}{2} \left(1 + \frac{\rho_2}{\rho_1}\right)}{D - h - \delta} + \frac{\Delta\rho}{\rho_1} \frac{T_1}{(D - h - \delta)^2}, \tag{A1}$$

where

$$T_1 = v(d_2 - \eta)(d_1 - h + \eta) + \frac{Q}{2} \left(\eta - d_2 + \frac{\rho_2}{\rho_1}(d_1 - h + \eta)\right), \tag{A2}$$

$$\delta = \frac{\Delta\rho}{\rho_1}(d_1 - h + \eta), \tag{A2}$$

$$a_{12} = \frac{(d_2 - \eta)(d_1 - h + \eta)}{D - h - \delta}, \tag{A3}$$

$$a_{21} = \frac{\Delta\rho g}{\rho_1} - \frac{v^2(d_2 - \eta + \frac{\rho_2}{\rho_1}(d_1 - h + \eta))}{(D - h - \delta)^2} + \frac{\Delta\rho}{\rho_1} \frac{T_2}{(D - h - \delta)^3}, \tag{A4}$$

where

$$T_2 = v^2 \left[ (d_2 - \eta)^2 - \frac{\rho_2}{\rho_1}(d_1 - h + \eta)^2 \right] + \frac{\rho_2}{\rho_1} Q \left( 2vD - \left(1 - \frac{\rho_2}{\rho_1}\right) Q \right), \tag{A5}$$

$$a_{22} = \frac{\left[ v \left( (d_2 - \eta)^2 - \frac{\rho_2}{\rho_1}(d_1 - h + \eta)^2 \right) + \frac{\rho_2}{\rho_1} Q(D - h) \right]}{(D - h - \delta)^2}. \tag{A6}$$

If one can make the assumption

$$\eta \frac{\Delta\rho}{\rho_1} \ll D - \frac{\Delta\rho}{\rho_1} d_1 - h \left( 1 - \frac{\Delta\rho}{\rho_1} \right), \tag{A7}$$

which implies  $\delta \approx \frac{\Delta\rho}{\rho_1}(d_1 - h)$ , and if  $h = 0$ , these reduce to

$$\eta \frac{\Delta\rho}{\rho_1} \ll D - \frac{\Delta\rho}{\rho_1} d_1, \text{ and } \delta \approx \frac{\Delta\rho}{\rho_1} d_1, \tag{A8}$$

the above expressions simplify to

$$a_{11} = \frac{v(d_2 - d_1 + h - 2\eta) + \frac{Q}{2} \left(1 + \frac{\rho_2}{\rho_1}\right)}{D - h - \delta}, \tag{A9}$$

$$a_{12} = \frac{(d_2 - \eta)(d_1 - h + \eta)}{D - h - \delta}, \tag{A9}$$

$$a_{21} = \frac{\Delta\rho g}{\rho_1} - \frac{v^2(d_2 - \eta + \frac{\rho_2}{\rho_1}(d_1 - h + \eta))}{(D - h - \delta)^2},$$

$$a_{22} = \frac{\left[ v \left( (d_2 - \eta)^2 - \frac{\rho_2}{\rho_1}(d_1 - h + \eta)^2 \right) + \frac{\rho_2}{\rho_1} Q(D - h) \right]}{(D - h - \delta)^2}, \tag{A10}$$

If we further make the Boussinesq approximation ( $\rho_2 = \rho_1$ , except for the first term in  $a_{21}$ ) we have

$$a_{11} = \frac{v(d_2 - d_1 + h - 2\eta) + Q}{D - h}, \tag{A11}$$

$$a_{12} = \frac{(d_2 - \eta)(d_1 - h + \eta)}{D - h}, \tag{A11}$$

$$a_{21} = \frac{\Delta\rho g}{\rho_1} - \frac{v^2}{D - h}, a_{22} = a_{11}. \tag{A12}$$